Physico-mechanical and Electrical Properties of NBR Structure Foams

A.M.Y. El-Lawindy

Department of physics, Faculty of Science, Suez Canal University, ISMAILIA, EGYPT

Nitrile butadiene rubber, NBR, structure foam of different apparent densities was obtained by using different concentrations of foaming agent, azodicarbonamide, ADC/K. The swelling factor in kerosene and benzene as a function of time was measured to elucidate the structure of these foams. This study was assisted by the current-voltage characteristics which were measured under the effect of different ratios of compressions: 0%, 10%, 30%, 40%, 50% and 60%. Under Joule heating limit, deviation of conductivity from Ohmic type of conduction, detected before, was observed as a result of compression. Shape factor, free current carrier mobility, and the equilibrium concentration of charge carrier in the conduction band were produced as functions of compressive strain. The conduction mechanism was found to follow the conventional band approach.

Introduction:

Most of the rubber foams uses have been derived from the desired combination of low density and some other physical properties. The dependence of physical properties on some parameters of polymeric materials is mainly empirical. On the other hand, the articles reviewed in foamed rubber physical properties are few. In a trial to explain the mechanical and electrical properties of EPDM and NBR foams with the existing theoretical models of unfoamed structure, recent works [1-2] have been published. The decrease of both mechanical and electrical properties upon foaming agent concentration was correlated with the decrease of the volume fraction of carbon black in the foamed rubber matrix. A linear relationship between volume fraction of carbon black and foaming agent concentration was found [1]. This result simplified the discussion of the mechanical properties in the light of the continuum mechanics theory for compressible materials [3-4].

The incorporation of gas cells inside rubber matrices will certainly affect the structure of carbon black as well as the cross-linking density in foamed rubber. The equilibrium between retraction forces which hold the rubber chains and the gas pressure experienced by a unit cross sectional area of the rubber matrix are responsible for such effect. This equilibrium is very sensitive to an internal pressure exerted by a suitable solvent or to an external pressure such as compression.

In a previous work [2], it was found that the conduction mechanism was ohmic up to ~ 400 volt. In the present work, the applied voltage was limited to 400 volt, and I-V characteristics were measured to examine the probable conduction mechanism changes under the application of different compressive strains.

Experimental Technique:

The foamed NBR rubber composite was compounded according to the recipe shown in Table 1. A two-roll mill was used. The ingredients were added in the same order as listed.

The specification of the two-roll mill used is as follow: length: 0.3 m, radius: 0.15 m, speed of slow roll: 18 rpm and gear ratio: 1.4. The compounded rubber was left for 24 hours before vulcanization.

Table (1): Ingredients of the investigated foamed NBR (N's) rubber composites.

Sample name Ingredients(phr)*	**N0**	**N5**	**N10**	**N15**	**Mixing time(min)**
NBR	**100**	**100**	**100**	**100**	10
Stearic acid	2	2	2	2	3
Zinc Oxide	5	5	5	5	5-7
HAF-N330	50	50	50	50	3-5
Processing oil	15	15	15	15	5
MBTS**	2	2	2	2	3
PBN***	1	1	1	1	3
Sulfur	2.5	2.5	2.5	2.5	5
ADC/K	**0**	**5**	**10**	**15**	6-8

* phr means part per hundred part of rubber by weight.
** MBTS is dibenzthiazole disulphide
*** PBN is phenyl-β-naphthyl amine

The specimens were compression molded into cylinders of 1 $x10^{-4}$ m^2 area and 0.01 m in height. The vulcanization were conducted under a heating press (KARL KOLB, Germany) at a pressure of P= 0.40 MPa. Many trials were conducted to obtain an optimum condition of temperature and time of vulcanization without samples being collapsed. The optimum conditions of temperature and time were T= 423 ^oK and t= 30 min. The vulcanized samples were shelf aged for 48 hours before test. The mixing time and vulcanization conditions were fixed for all samples. Brass electrodes were attached to the parallel faces of samples during vulcanization. Material tester (AMETEK, USA) was facilitated in this experiment. A digital force gage (Hunter Spring ACCU Force II, 0.01 N resolution, USA) of 50 N capacity was used to measure stress forces. In electrical measurements a digital electrometer (616 Kiethly, USA) and a RCL bridge (3531 Z-Hitester,Hioki, Japan) was used.

Results and Discussion:

Figure (1) depicts the behavior of swelling factor, Q%, as a function of swelling time, t (hr), in benzene and kerosene respectively. In general, one may notice that the swelling in benzene is higher than that in kerosene due to the different molecular size of both solvents. The smaller the solvent molecule the larger the diffusion rate, [5-6]. In addition, it was found that Q% increases by increasing the foaming agent concentration. The increase of Q% with foaming agent concentration may be attributed to extra internal forces imposed by the gas cells in addition to the internal forces exerted by solvents.

A close inspection of the swelling behavior shows no smooth variation of Q% with time, especially for foamed samples. There are abrupt changes in the curve, that increase by increasing foaming agent concentration, C_f. These

abrupt changes may be attributed to a break up of some cross-links due to the extra internal energy imposed by gas cells and solvent. The equilibrium-swelling factor has not been achieved until the end of the measuring time, 48 hr, indicating continuos break up of cross-links.

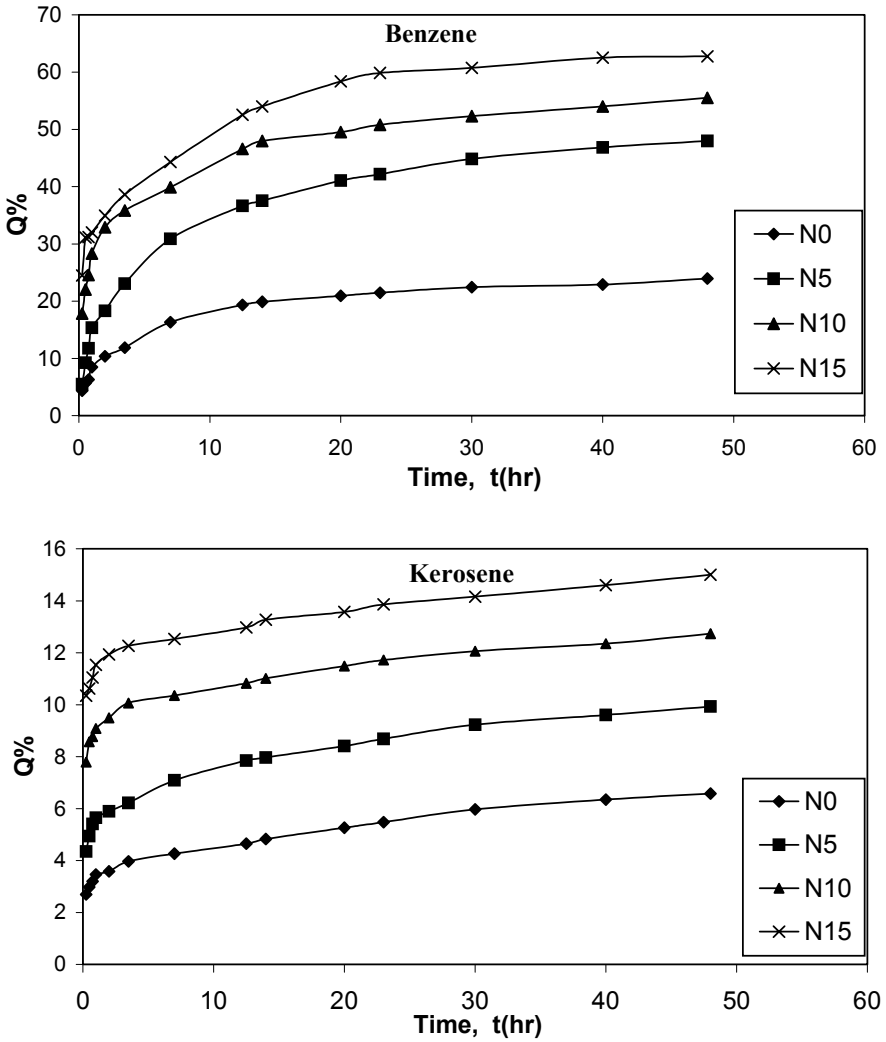

Fig. (1): Swelling factor, Q%, as a function of time of swelling in benzene and kerosene.

The average characteristic times, τ, of swelling in NBR foams as a function of C_f is depicted in Fig. (2). It shows a slower τ or faster equilibrium as the C_f is increasing.

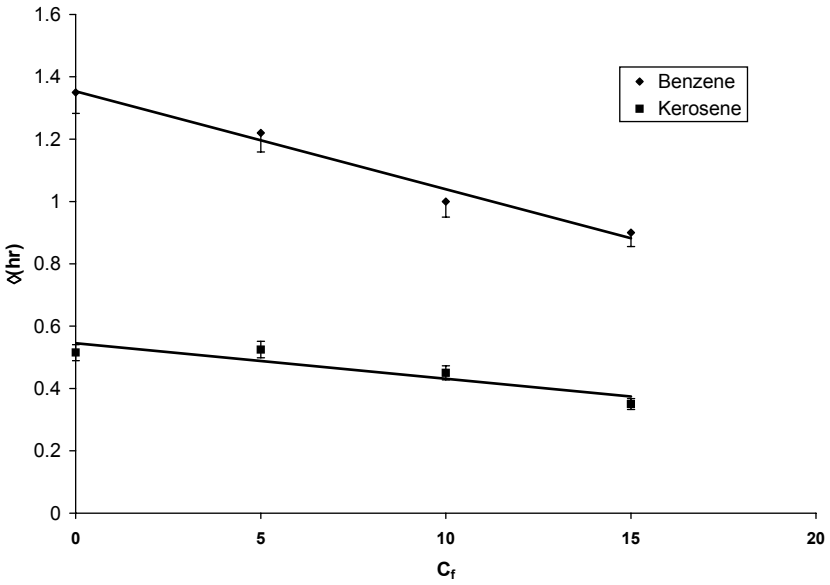

Fig. (2): The characteristic swelling time, τ(hr) as a function of HAF-N330 carbon black volume fraction, C_f.

Figure (3) shows the conductivity measured at room temperature, ~300 K, as a function of compressive strain ratio and foaming agent concentration. In general one observes a decrease in conductivity as the foaming agent concentration is increased. For foam free samples one notices a sharp decrease in conductivity followed by a slight increase upon the application of strains. The initial decrease may indicate carbon black aggregation collapse that followed by reformation as the volume decreases under the effect of compressive strain. For foams, it was seen that the conductivity decreases as the compressive strain increases up to ~30% after which the conductivity became strain independent. It should be emphasized that it is more difficult to collapse the cell structure in the thickness direction. Consequently, one expects the motion of aggregates to be in the lateral direction between gas cells. This may explain the initial decrease in conductivity. This assumption may be confirmed by calculating the shape factor of carbon filler by using a modified Guth [7] equaion:

$$\sigma_s/\sigma_o = 1 - f\phi_c - f^2\phi_c^2 \qquad (1)$$

where σ_o is the initial conductivity, σ_s is the conductivity under strain, f is the shape factor, and ϕ_c is the volume fraction of carbon filler. The positive signs in

Guth equation are replaced by negative signs to account for the decrease of conductivity due the increase of foaming agent concentration. Fig. (4) depicts the calculated *f*-values as a function of compressive strains. It is noticed that the shape factor is sensitive to compression. The effect of foaming agent concentration on shape factors was previously calculated [1]. It was found that as foaming agent increased the shape factor increased resulting in a change from rod like to oblate shape, then to prolate without passing through a spherical shape. Under compressive strains, the measured *f*- values indicate an

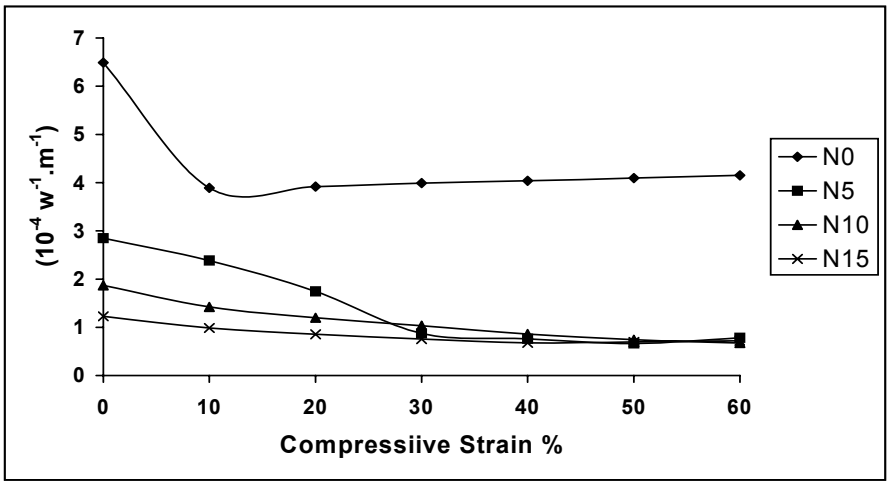

Fig. (3): The electrical conductivity, σ_m, as a function of compressive strain ratio for all samples, N0, N5, N10, N15.

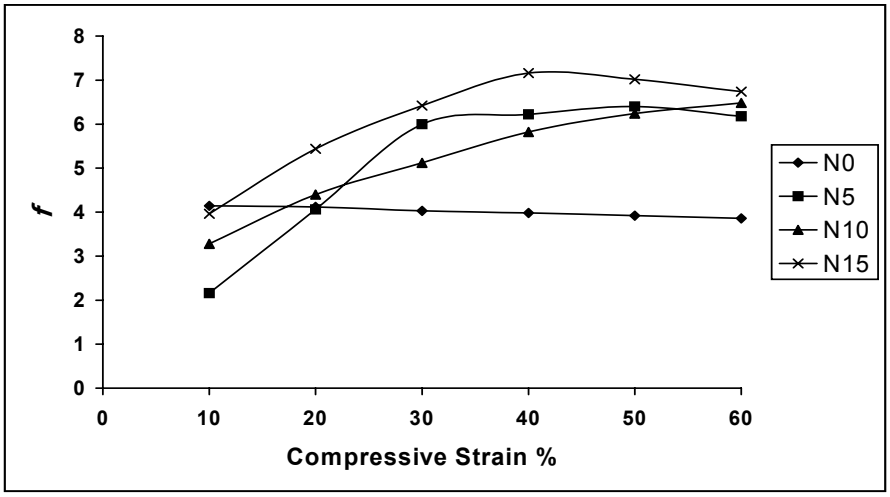

Fig. (4): The calculated shape factor, *f*, as a function of compressive strain ratio for all samples, N0, N5, N10, N15.

abrupt change to prolate shape upon immediate application of strains. It is increasing up to ~40% strain, after which it became strain independent. This may indicate that the carbon aggregates are arranged in planner surfaces perpendicular to the direction of compressive forces. These surfaces are partially connected to each other by dispersed smaller aggregates that are responsible for the conduction occurred. This may explain the conductivity strain independent above ~40% strain.

To account for this behavior, the current -voltage, (I-V) characteristics were measured, Fig. (5), at different compression deformation. Fig. (6) shows the plot of the current, I, as a function of the square of the applied voltage, V^2, for the whole region of the applied field. Above ~200 volt, it is seen that the behavior is linear, indicating space charge conduction beyond ~200 volts. The relation of current density (J) in the square law region is given, [8-12] by:

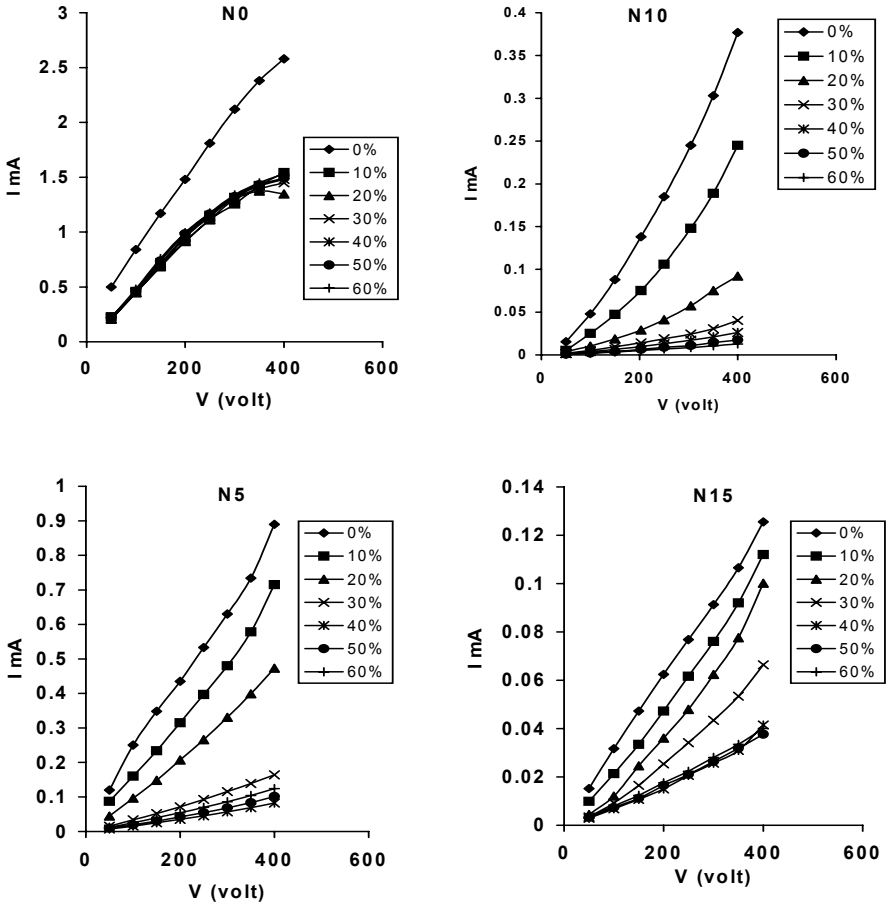

Fig. (5): The current-voltage characteristics, I-V, as a function of compressive strain ratio for all samples, N0, N5, N10, N15.

$$J=9\varepsilon\varepsilon_o\mu_o V^2/8a^2 \quad (2)$$

where μ_o is the free carrier mobility, ε_o, the permittivity of free space, ε, the dielectric constant of the sample material, measured at 1000 Hz, and a is the sample thickness. The formation of space-charge is due to the existence of some traps within that composites that can occur at particular molecular sites and chain folds [13]. When a trap level exists, the mobility is reduced by $1/\theta$, and the effective electron drift mobility, μ_e, in an insulator with traps is therefore

$$\mu_e = \mu_o\,\theta \quad (3)$$

where θ is the trapping factor. Therefore, in the trap-square law region, the relation between J and V^2 becomes [9,11,12]

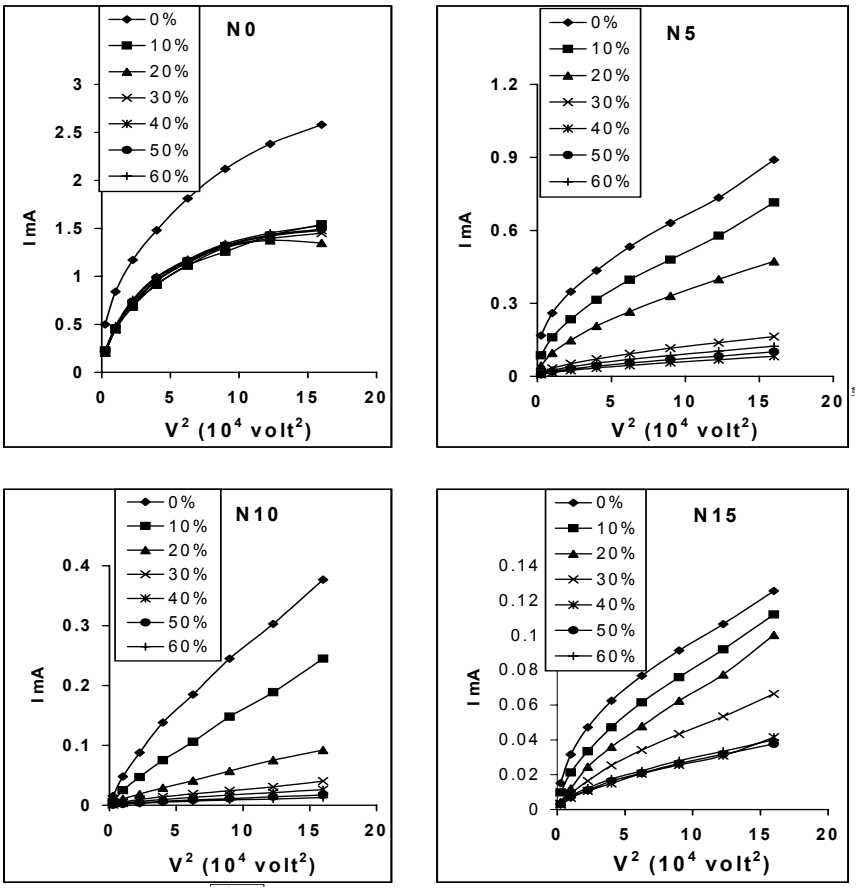

Fig. (6): The I-V^2 plots as a function of compressive strain ratio for all samples, N0, N5, N10, N15.

$$J=9\varepsilon\varepsilon_o\mu_e V^2/8\theta a^2 \quad (4)$$

The free carrier mobility, μ_o, can be calculated at different deformations using the experimental value of θ and the slope of (I-V^2) plots. Experimentally, θ is the ratio between the current densities at the beginning I_1 and at the end I_2 of the trap-square law region. Also θ is the ratio between the free electron concentration, n_o, in the conduction band to the total electron density, n_o+n_t , n_t being the density of trapped electron. Thus

$$I_1/ I_2 =\theta = n_o/(n_o+n_t) \quad (5)$$

The equilibrium concentration of the charge carrier in the conduction band, n_o, can also be obtained using the relation [10]

$$n_o=(\varepsilon\varepsilon_o\theta/qa^2)V_{tr} \quad (6)$$

where q is the electron charge and V_{tr} is the voltage at which the transition from the ohmic to square law region takes place. Note that n_t can also be calculated. For one type of current carrier, the conductivity, σ, is given by:

$$\sigma = qn_o\mu_o \quad (7)$$

In table 2, the produced values of θ, $\mu_e(m^2V^{-1}s^{-1})$, μ_o $(m^2V^{-1}s^{-1})$, $n_e(m^{-3})$, $n_o(m^{-3})$, $\sigma(\Omega.m)^{-1}$, and $\sigma_m,(\Omega.m)^{-1}$ are presented, where σ_m is the measured conductivity determined from the ohmic region. The last column presents the ratio between the calculated conductivity, eq. 7, to that obtained from the experimental data σ_m. A fair consistency between measured and calculated conductivity is observed.

Figure (7) depicts the behavior of μ_o $(m^2V^{-1}s^{-1})$ as a function of compressive strain ratios. One notices that μ_o is sensitive to foaming agent concentration above 5 phr foams. In addition the effect of compressive strain on μ_o predominates up to ~30% compression, after that μ_o become compression independent. Fig. (8) depicts the calculated values of carrier concentration, n_o at different compressive strain ratios. It is seen that n_o values are compression independent. It is interesting to note that only the variation of μ_o with compression is responsible for the observed change of conductivity. It was established [14] that if μ_o is greater than 10^{-4} $m^2V^{-1}s^{-1}$ the conduction mechanism is a conventional band model. The calculated μ_o values of Table (2) show that the conduction mechanism belongs to the conventional band model.

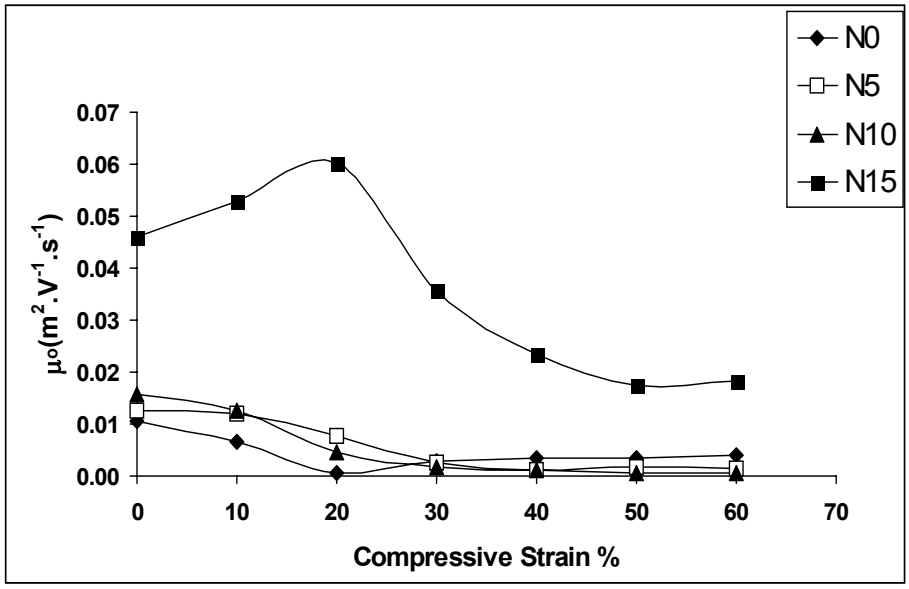

Fig. (7): The calculated free carrier mobility, μ_o, as a function of compressive strain ratio for all samples, N0, N5, N10, N15.

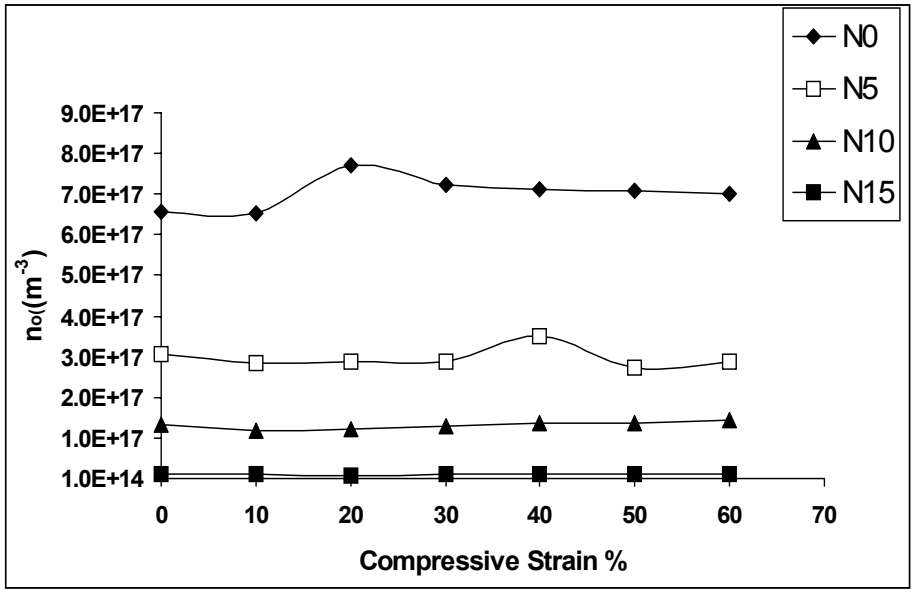

Fig. (8): The calculated free carrier density, n_o, as a function of compressive strain ratio for all samples, N0, N5, N10, N15.

Sample Name: **N0**

Compres.	slope	ε	μ_ε	θ	n_o	n_t	μ_o	σ	σ_μ	ratio
0%	6.5E-09	3.7E+03	8.6E-03	0.82	6.6E+17	1.4E+17	1.0E-02	1.1E-03	6.5E-04	1.70
10%	4.1E-09	3.7E+03	5.3E-03	0.81	6.5E+17	1.5E+17	6.6E-03	6.8E-04	3.9E-04	1.76
20%	4.9E-10	3.7E+03	6.5E-04	0.96	7.7E+17	3.0E+16	6.7E-04	8.3E-05	3.9E-04	0.21
30%	2.0E-09	3.7E+03	2.7E-03	0.90	7.2E+17	7.8E+16	2.9E-03	3.4E-04	4.0E-04	0.85
40%	2.3E-09	3.7E+03	3.0E-03	0.89	7.1E+17	8.8E+16	3.4E-03	3.9E-04	4.0E-04	0.96
50%	2.3E-09	3.7E+03	3.0E-03	0.89	7.1E+17	9.0E+16	3.4E-03	3.8E-04	4.1E-04	0.94
60%	2.7E-09	3.7E+03	3.6E-03	0.88	7.0E+17	9.9E+16	4.1E-03	4.5E-04	4.2E-04	1.10

N5

Compres.	slope	ε	μ_ε	θ	n_o	n_t	μ_o	σ	σ_μ	ratio
0%	3.6E-09	2.4E+03	7.5E-03	0.60	3.1E+17	2.0E+17	1.2E-02	6.1E-04	2.8E-04	2.14
10%	3.2E-09	2.4E+03	6.7E-03	0.56	2.8E+17	2.3E+17	1.2E-02	5.5E-04	2.4E-04	2.29
20%	2.1E-09	2.4E+03	4.4E-03	0.56	2.9E+17	2.2E+17	7.8E-03	3.6E-04	1.7E-04	2.04
30%	7.3E-10	2.4E+03	1.5E-03	0.57	2.9E+17	2.2E+17	2.6E-03	1.2E-04	8.7E-05	1.40
40%	3.8E-10	2.4E+03	7.8E-04	0.69	3.5E+17	1.6E+17	1.1E-03	6.4E-05	7.6E-05	0.83
50%	4.8E-10	2.4E+03	9.8E-04	0.54	2.7E+17	2.4E+17	1.8E-03	8.0E-05	6.7E-05	1.20
60%	3.8E-10	2.4E+03	7.8E-04	0.56	2.9E+17	2.2E+17	1.4E-03	6.4E-05	7.8E-05	0.81

N10

Compress.	slope	ε	μ_ε	θ	n_o	n_t	μ_o	σ	σ_μ	ratio
0%	2.0E-09	1.3E+03	7.7E-03	0.49	1.1E+17	1.1E+17	1.6E-02	2.7E-04	1.9E-04	1.44
10%	1.4E-09	1.3E+03	5.5E-03	0.43	9.4E+16	1.2E+17	1.3E-02	1.9E-04	1.4E-04	1.34
20%	5.4E-10	1.3E+03	2.1E-03	0.45	9.7E+16	1.2E+17	4.6E-03	7.2E-05	1.2E-04	0.60
30%	2.2E-10	1.3E+03	8.4E-04	0.47	1.0E+17	1.2E+17	1.8E-03	2.9E-05	1.0E-04	0.28
40%	1.4E-10	1.3E+03	5.3E-04	0.50	1.1E+17	1.1E+17	1.1E-03	1.8E-05	8.6E-05	0.21
50%	9.1E-11	1.3E+03	3.5E-04	0.50	1.1E+17	1.1E+17	7.0E-04	1.2E-05	7.5E-05	0.17
60%	6.5E-11	1.3E+03	2.5E-04	0.53	1.2E+17	1.0E+17	4.7E-04	8.7E-06	6.8E-05	0.13

N15

Compres.	slope	ε	μ_ε	θ	n_o	n_t	μ_o	σ	σ_μ	ratio
0%	5.2E-10	8.9E+01	2.8E-02	0.61	9.5E+15	6.0E+15	4.6E-02	7.0E-05	1.2E-04	0.57
10%	5.3E-10	8.9E+01	2.9E-02	0.55	8.5E+15	6.9E+15	5.3E-02	7.2E-05	9.9E-05	0.72
20%	5.3E-10	8.9E+01	2.9E-02	0.48	7.4E+15	8.1E+15	6.0E-02	7.1E-05	8.6E-05	0.83
30%	3.4E-10	8.9E+01	1.8E-02	0.52	8.0E+15	7.5E+15	3.6E-02	4.5E-05	7.6E-05	0.60
40%	2.1E-10	8.9E+01	1.2E-02	0.50	7.7E+15	7.8E+15	2.3E-02	2.9E-05	6.8E-05	0.42
50%	1.8E-10	8.9E+01	9.7E-03	0.56	8.6E+15	6.8E+15	1.7E-02	2.4E-05	7.0E-05	0.34
60%	1.9E-10	8.9E+01	1.0E-02	0.56	8.6E+15	6.9E+15	1.8E-02	2.5E-05	7.2E-05	0.35

Conclusion:

Foamed NBR were prepared using a simple technique. The swelling in benzene and in kerosene shows the effect of gas cells and solvents. They exert an extra internal force that results in a break up of some cross-links of the host matrix.

The internal structure of carbon black was affected by the compressive strains. The measured I-V characteristics show deviation from ohmicity upon compressive deformation of samples. The conductivity shows a dramatic decrease as the applied deformation increases up to ~40% after which it became deformation independent. These changes may be attributed to the change of carbon black structure as well as the lateral deformation of gas cells. This assumption was confirmed by calculating the shape factor of carbon black filler.

The carrier concentration in conduction band was found compression deformation independent. The variation of the free carrier mobility was found sensitive for both foam concentration above 5phr and compressive strains up to 30%. Consequently, the change in mobility is responsible for the change in conductivity. The calculated μ_o values show that the conduction mechanism belongs to the conventional band model.

References:

1. A.M.Y. El-Lawindy, K.M. Abdel-Kader, W.E. Mahmoud and H.H. Hassan; *Polym. Int*.Vol., **51,** 7, 601 (2002) .

2. A.M.Y. El-Lawindy, W.E. Mahmoud and H.H. Hassan; The XXIII Conference on Solid State Science, 28 th Sep. –2 nd Oct. (2002), Sharm El-Shiekh, Sinai, Egypt.

3. L.E Nielsen, R.F. Landel, "Mechanical Properties of Polymers and Composites", Marcel Dekker, Inc., New York, Basel, Hong Kong (1994).

4. A.E. Green, and J.E Adkins", *Large Elastic Deformation and Non-linear Continuum Mechanics"*, Clarendon press, Oxford, (1960).

5. A. Tager, "*Physical Chemistry of Polymers*", Mir Publ. Moscow (1972)

6. T. Whelan, "*Polymer Technology Dictionary*", Chapman & Hall, London, (1994)

7. E.Guth, *J.Appl. Polys*, **16,** 20 (1945).

8. D.A. Seanor, "*Electrical Properties of Polymers*", Academic Press, New York, London, p. **34** (1982).

9. A.D.Jenkins, "*Polymer Science*", North Holland, Amsterdam, London, p. 1210 (1972).

10. J. Chutia and K. Barua, *J. Phys. D Appl. Phys*., 1**3**, 9 (1980).

11. M.A. Lampert, *Phys. Rev*., 103, 1648(1956);

12. M.A. Lampert, *Proc. I.R.E*., **50,** 1781 (1962).

13. S.H. Glarium, *J. Phys. Chem.Solids*, **24,** 1577 (1963).

14. A. R. Blythe, "*Electrical Properties of Polymers*"; Cambridge University Press, Cambridge, (1980).